

# Enhancing ambient temperature grain boundary plasticity by grain refinement in bulk magnesium

Hidetoshi Somekawa<sup>\*</sup>, Masato Wakeda<sup>\*\*</sup>, Alok Singh

Research Center for Structural Materials, National Institute for Materials Science, 1-2-1 Sengen, Tsukuba, Ibaraki, 305-0047, Japan

## ARTICLE INFO

### Keywords:

Magnesium  
Grain boundary  
Diffusivity  
Activation energy  
Strain rate sensitivity  
Deformation mechanism

## ABSTRACT

Room temperature ductility of magnesium is known to be dramatically enhanced by partial contribution of grain boundary sliding. However, the effect of grain size on grain boundary plasticity as well as accommodation process for this unique room temperature grain boundary sliding are unclear. In this study, tensile tests at ambient temperatures and detailed deformed microstructural observations are performed to investigate these points using extruded magnesium of average grain sizes between 1  $\mu\text{m}$  and  $\sim 50 \mu\text{m}$ . The results of tensile tests exhibit that elongation-to-failure in tension and deformation mechanism vary with grain sizes. Fine-grained magnesium (in orders of several micrometer) shows the elongation-to-failure in tension of  $\sim 100\%$  with activation energy of 80 kJ/mol, which is close to grain boundary diffusion of magnesium. This high ductility results from grain boundary sliding accommodated with dislocation slip by diffusion process. Accordingly, the ductility and activation energy reduces with grain size coarsening. Deformed microstructural observations using EBSD and TEM display the activation of non-basal dislocations at grain boundaries. Specific regions in geometrically necessary dislocation map of grain interior consisting of meso- and coarse-structures ( $> 10 \mu\text{m}$ ) show a high value, which suggests the presence of strains. Moreover, the formation of sub-grain boundaries is confirmed in grain interior of coarse-grained structure. This is attributed to dominant occurrence of intragranular deformation mode, associated with insufficient diffusivity, such as grain boundary diffusion.

## 1. Introduction

Grain boundaries of magnesium (Mg) and its alloys have unique characteristics and affect plastic deformation behavior. It is well-recognized that the major slip system in single crystals is basal at low- and room-temperatures, because of a large difference in critical resolved shear stress (CRSS) between the basal and non-basal planes. In polycrystals, on the other hands, the basal slips as well as non-basal dislocation slips are activated in the vicinity of grain boundaries, owing to operating compatibility stress at these grain boundaries [1]. As a result, wrought-processed common Mg alloys with meso-grained structures (grain size of  $\sim 10\text{--}30 \mu\text{m}$ ) exhibit strain hardening behavior and elongation-to-failure in tension of  $\sim 20\text{--}30\%$  [1–3]. In these alloys, the fracture is unlikely to show brittleness but is likely to have a ductile pattern associated with micro-void coalescence.

From another point of view, the coefficient of grain boundary diffusion,  $1 \times 10^{-2} \text{m/s}$ , of this pure metal is larger than that of the other metallic material, for instance,  $1 \times 10^{-4} \text{m/s}$  in the competing light-

weight metallic material, aluminum (Al) [4]. This especially suggests that grain boundary diffusivity is highly likely to influence plastic deformation in Mg at not only intermediate but also ambient temperatures. Regarding the deformation behavior at intermediate temperatures (in particular between  $\sim 373 \text{K}$  and  $473 \text{K}$ ), several studies on Mg alloys have shown a low temperature superplastic behavior, where it is noted that grain boundary sliding is the rate-controlling deformation mechanism [5–13]. Mabuchi et al. have reported a low temperature superplasticity, where a fine-grained AZ91 alloy exhibits an elongation-to-failure of  $\sim 1000\%$  at  $473 \text{K}$  in a strain rate of  $1 \times 10^{-4} \text{/s}$  [11]. Watanabe et al. have pointed out that suitable temperatures to obtain a large ductility in superplastic Mg alloys are much lower than those for the superplastic Al alloys [13]. As for the deformation behavior at room temperature, Wang et al. have reported that the  $m$ -value (where the  $m$ -value is the term of creep equation (1) in later section, 4.2) is obtained to be 0.25 in two types of measurement methods, i.e., nano-indentation creep test and uniaxial tensile test, using fine-grained bulk Mg metal [14]. The results obtained from

<sup>\*</sup> Corresponding author.

<sup>\*\*</sup> Corresponding author.

E-mail addresses: [SOMEKAWA.Hidetoshi@nims.go.jp](mailto:SOMEKAWA.Hidetoshi@nims.go.jp) (H. Somekawa), [WAKEDA.Masato@nims.go.jp](mailto:WAKEDA.Masato@nims.go.jp) (M. Wakeda).

nano-indentation creep tests have shown that the vicinity of grain boundaries has a high strain rate sensitivity, i.e.,  $m$ -value of 0.5, whereas the  $m$ -value goes down to  $\sim 0.1$  far from the grain boundaries [15]. This localized deformation response implies that grain boundary sliding easily occurs at/around grain boundaries even at room temperature. Koike et al. have confirmed that the trace lines drawn by focused ion beam method mismatch at grain boundaries in the tensile tested Mg alloy, due to the occurrence of grain boundary sliding [16]. These results suggest that introducing a high volume fraction of grain boundaries is able to cause an increase in contribution of grain boundary plasticity to deformation.

Regarding the characteristics of fine-grained Mg and its alloys [17–19], recent studies have reported that the elongation-to-failure in tension exceeds 200% in an average grain size of approximately 1  $\mu\text{m}$  in low strain rate regimens [20]. With a focus on the quasi-static strain rates, the tensile elongations are obtained to be 65% for the Mg metal with an average grain size of 0.65  $\mu\text{m}$  [21] and 170% for the Mg–Bi binary alloy with 1.2  $\mu\text{m}$  [22], which are found to be much superior to those of common Mg alloys. Several deformed microstructural observations have also shown that such a huge ductility results from grain boundary sliding [20,22,23], and the contribution of this deformation mechanism increases with grain refinement [24].

Nevertheless, it is known that stress concentration owing to grain boundary sliding takes place at triple points and/or grain boundary interfaces, which become the origin of fracture [25–29]. As in the conventional superplastic flow, cavitation is also observed to be formed during room temperature grain boundary sliding [30]. In this case, the accommodation process is necessary to attain a large ductility associated with grain boundary sliding. It has been well accepted that an accommodation processes for grain boundary sliding is diffusion-controlled dislocation slip under “the general condition” for superplastic flow to occur [31–33]. Regarding room temperature grain boundary sliding, some of thermomechanical analysis studies have displayed that the activation energies obtained from tensile/compressive tests at ambient and intermediate temperatures are similar to that of grain boundary diffusion in Mg metal [19,20,22]. All of these studies are focused on the fine-grained Mg metals associated with a high density of grain boundaries. The possible influential factors for accommodation mode based on in-situ and ex-situ microstructural observations have also been discussed [18]. While they have proposed a combined process of grain rotation and dislocation slip, there are few considerations of diffusivity to accommodation mode [18]. Under these situations, there still remains an unclear point about the influence of grain boundary plasticity including diffusivity on deformation. Therefore, in this study, to understand the role of grain boundaries, we have systematically inspected the uniaxial tensile behavior at ambient temperatures including a low temperature of 273 K in low strain rate regimens using various bulk specimens with different grain sizes. We have also considered the effect of grain size on accommodation process for this unusual room temperature grain boundary sliding.

## 2. Experimental procedures

Commercial grade pure Mg metal (purity of 99.96 mass%) with different average grain sizes was used in this study. Cast Mg was extruded to reduce casting defects and to produce fine-, meso- and coarse-grained structures (average grain size of  $\sim 1$ –50  $\mu\text{m}$ ) at temperatures between 378 K and 628 K with an extrusion ratio of 25:1 at an extrusion speed of 0.2 mm/s. Microstructures of these extruded Mg metals were observed by the electron backscattered diffraction (EBSD) method in a scanning electron microscopy (SEM). These EBSD data were analyzed through EDAX/TSL software to obtain the average grain size, as well as the basal texture (i.e., the (0001) plane orientation distribution). Grain size obtained from this analysis is used as the initial condition prior to deformation. Basal texture was also evaluated by the Schultz reflection method using Cu-K $\alpha$  radiation. The observed regions

for both EBSD and Schultz reflection methods were planes with a normal to extrusion direction. In order to investigate the thermomechanical behavior, uniaxial tensile tests were performed at three kinds of temperatures (low temperature (273 K), room-temperature (298 K) and intermediate temperature (323 K)) in low strain rate ranges. The initial strain rates were selected to be  $1 \times 10^{-4}$  and  $1 \times 10^{-5}$ /s at the temperatures of 298 and 323 K. It is noted that a jump test was performed to acquire the  $m$ -value at low temperature conditions, due to the limitation of cooling system in this facility. In the jump test, the tensile strain rate was changed from  $1 \times 10^{-5}$  to  $1 \times 10^{-4}$ /s on reaching nominal strain of 0.125. In case of the extruded Mg metals with meso- and coarse-grains, since a ductility above 12.5% was not obtained at 273 K in both strain rates, the constant tensile tests were conducted as an alternative to the jump tests. Specimens were held for at least 300 s at low and intermediate temperatures before the tensile tests. Tensile specimens had a cylindrical dog-bone shape with a gauge length of 10 mm and a gauge diameter of 2.5 mm. They were prepared by lathe turning machine parallel to the extrusion direction. The tensile tests were performed in at least triplicate under specific conditions, i.e., at 298 K and 323 K, to confirm the repeatability using the meso-grained Mg metals. The difference in elongation-to-failure in tension had a few percent associated with the existence of internal defects; however, flow stress showed similar results in each test.

In specific extruded Mg metals, microstructures in the same region before and after tensile testing were observed by EBSD with a scanning step size of less than 50 nm. These deformed specimens were prepared by applying a tensile strain of 0.10 at room temperature in  $1 \times 10^{-5}$ /s. In addition, transmission electron microscopy (TEM) was used to further observe the microstructures in specific regions (A and E), as marked in Fig. 6(c), in the above-mentioned deformed specimen. The specimens for TEM observations were prepared by focused ion beam (FIB) machining technique in SEM. Besides the conventional TEM technique, scanning TEM (STEM) mode was also used with large camera length to image strain contrast. Deformed internal microstructure and surface features of after-fractured specimens were additionally observed by EBSD and SEM. Fine- and meso-grained Mg metals (grain size of 2.6  $\mu\text{m}$  and 17.2  $\mu\text{m}$ ) tested at 298 K and  $1 \times 10^{-5}$ /s were selected for SEM observations and both observations, respectively. All specimens for the EBSD observations in the as-extruded Mg metals and deformed samples were prepared by polishing under SiC paper, diamond slurries with 9  $\mu\text{m}$  and 1  $\mu\text{m}$  and alumina slurry, then, were etched using acid solution (10 mL HNO<sub>3</sub>, 30 mL acetic acid, 120 mL ethanol and 40 mL H<sub>2</sub>O) for several seconds. It is to be noted that the plate shaped dog-bone tensile specimens were used in these experiments for microstructural evolutions before and after testing. The dimension was the length of 8 mm, the width of 2 mm and the thickness of 1 mm. They were also prepared by milling machine, and the tensile direction was parallel to extrusion direction, which is the same as that in cylindrical shaped specimens.

## 3. Results

Inverse pole figure images from EBSD observations of the extruded Mg metals are shown in Fig. 1. Microstructures consist of recrystallized structures without any presences of deformation twins, regardless of the extrusion temperatures. Fig. 1(h) is the cumulative fraction in grain size of each extruded Mg metal obtained from EBSD results. There are some scatters associated with presence of a few mixed structures, but the distribution in grain size tends to increase monotonically. Average grain sizes including standard deviation obtained from the EBSD analysis are listed in Table 1. Extrusion process at lower temperature leads to finer-grained structures. The average grain sizes exist in between 1.5  $\mu\text{m}$  and  $\sim 50$   $\mu\text{m}$ . Table 1 also includes the analysis results about misorientation features. The extruded Mg metals have similar average misorientation angles of approximately 40°, which are similar in values to the previous results of wrought-processed Mg alloys [34]. The volume fractions of low-angle grain boundaries ( $4^\circ < \theta < 15^\circ$ , where  $\theta$  is the

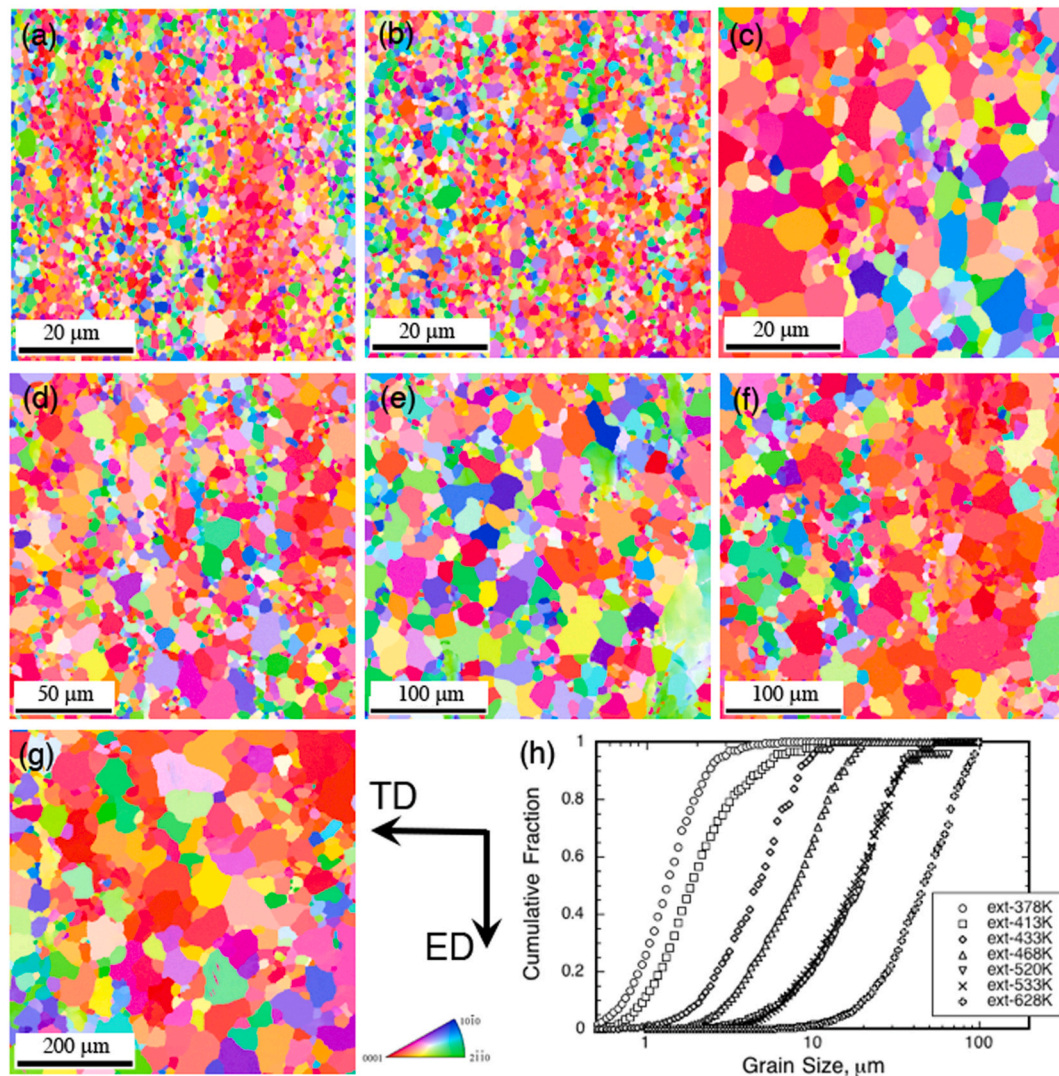


Fig. 1. (a) inverse pole figure image in the extruded Mg metal at extrusion temperature of 378 K, (b) 413 K, (c) 433 K, (d) 468 K, (e) 520 K, (f) 533 K and (g) 628 K, and (h) cumulative fraction in grain size obtained from EBSD results. where TD and ED indicate the transverse- and extrusion-directions, respectively.

Table 1

The results of microstructural observations and tensile tests in the extruded Mg metals.

$T_{\text{ext}}$ , K	$d$ , $\mu\text{m}$	$\theta$ , $^{\circ}$	$V_{\text{LAG}}$ , %	SF	$m$ -value	$Q$ , kJ/mol	$m_{\text{L}}$ -value	$m_{\text{H}}$ -value
378	$1.5 \pm 0.7$	39.9	10.0	0.18	0.219	79.0	0.122	0.326
413	$2.6 \pm 2.0$	43.8	8.6	0.20	0.104	64.8	0.067	0.232
433	$5.1 \pm 2.7$	38.7	9.1	0.16	0.107	45.0	0.057	0.133
468	$8.6 \pm 4.6$	40.3	9.6	0.21	0.078	40.2	0.052	0.131
520	$17.2 \pm 13.1$	41.6	10.2	0.19	0.071	30.9*	0.038*	0.092
533	$20.0 \pm 11.6$	40.2	10.8	0.20	0.035	29.8*	0.031*	0.095
628	$50.2 \pm 23.5$	41.4	11.8	0.22	0.026	—	—	0.059

Where  $T_{\text{ext}}$  is the extrusion temperature,  $d$  is the average grain size,  $\theta$  is the average misorientation angle,  $V_{\text{LAG}}$  is the volume fraction of low-angle grain boundaries,  $Q$  is the activation energy, which is shown typical examples for calculation method as Fig. 13. SF indicates Schmid factor of  $\langle 11\bar{2}0 \rangle$  (0001) obtained from EBSD results using EDAX analysis software. Each  $m$ ,  $m_{\text{L}}$  and  $m_{\text{H}}$ -value are obtained from room-, low- and intermediate temperatures (298, 273 and 323 K) tensile tests. As for star marks, it is noted that activation energies and the  $m_{\text{L}}$ -values in extruded Mg metal with grain sizes of 17.2 and 20  $\mu\text{m}$  are obtained through flow stress of nominal strain of 0.05, due to insufficient ductility of less than 10%.

misorientation angle) are 0.10 (10%) in all the Mg metals. The fraction of low-angle grain boundaries is also unlikely to depend on the extrusion temperatures. In Figs. 1(a)–(g), these extruded Mg metals are also found to have a basal texture. The results of (0001) pole figure measured through the Schultz reflection method are shown in Fig. 2. The same as the results in the EBSD observations, grains orient on the (0001) plane

parallel to the extrusion direction, due to the hot extrusion. It is noted that the Mg metals extruded at high temperatures show high maximum intensity but weaken the basal texture. This resulted from the numbers of grain in the measurement area: the fraction/density of grains is low in the coarse-grained Mg metals. In the case of existence of specific coarse grains having a strong texture, the intensity is influenced by these

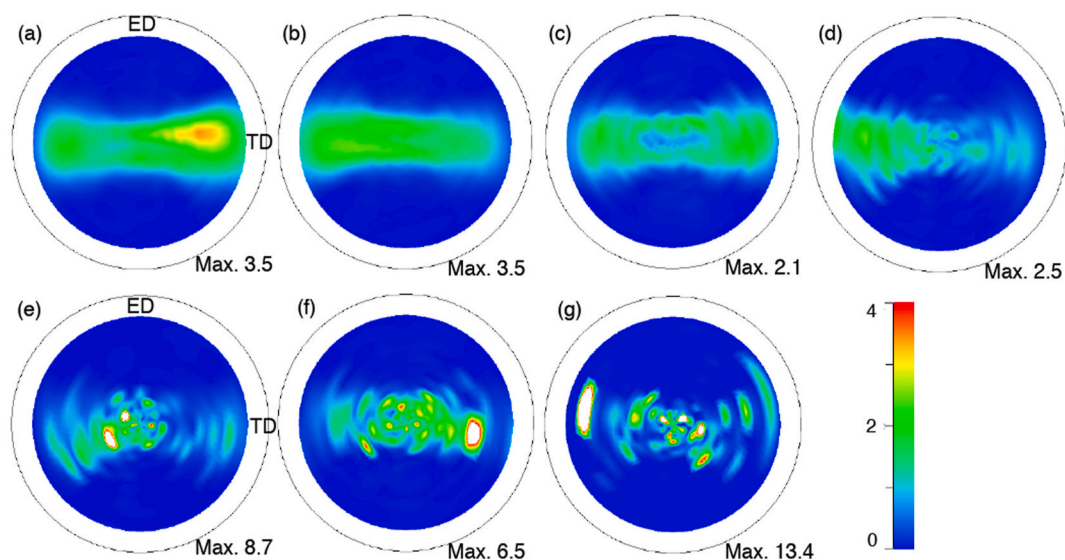


Fig. 2. (0001) pole figure images taken by Schultz reflection method in the extruded Mg metals: (a) extrusion temperature of 378 K, (b) 413 K, (c) 433 K, (d) 468 K, (e) 520 K, (f) 533 K and (g) 628 K, where TD and ED indicate the transverse- and extrusion-directions, respectively.

grains, and the texture features seem to be weakening. In order to confirm the texture feature, Table 1 includes the Schmid factor of  $\langle 11\bar{2}0 \rangle(0002)$ , i.e., basal plane, obtained from EBSD analysis. Schmid factors in these extruded Mg metals are 0.15–0.21, being similar, irrespective of grain size (extrusion temperature). These results and analyses display that the extruded Mg metals have a similar texture.

Nominal stress vs. strain curves of tensile tests at room temperature in the extruded Mg metals are shown in Fig. 3. The stress vs. strain curves at low and intermediate temperatures are provided in Figs. 4 and 5, respectively. The scale on the y-axis is the same in all the curves to allow for easy comparison. Fig. 4(a) shows the results obtained from the common tensile tests in the initial strain rate of  $1 \times 10^{-4}/s$ , and includes the results of the jump test using fine-grained Mg metal to compare with stress vs. strain behaviors in two types tests. These curves are found to overlap, which suggests the same deformation occurs, regardless of the evaluation methods. In Fig. 4(b), some of Mg metals exhibit low ductility, but flow stress apparently increases at the strain of 0.125 associated with testing methods. Regarding Figs. 3–5, tensile behaviors are influenced by internal and external factors, such as grain size, tensile testing temperature and strain rate. The flow stress decreases with lower strain rates at any tensile temperatures between 273 K and 323 K. On the

contrary, it is interesting to notice that yield strength of the fine-grained Mg metals tends to show a decrease, when the grain size becomes finer than  $\sim 5 \mu m$ , as well-recognized as the inverse Hall-Petch relation. In Figs. 4 and 5, this relation is also confirmed at both low and intermediate temperatures (273 K and 323 K). This unusual Hall-Petch behavior of Ni and Cu metals is observed in the grain size of nanometer orders (typically less than 10 nm) [35–40]; while, for Mg metal, it is at least three or four magnitudes of coarser-grained structures. Similarly, grain size and strain rate affect the elongation-to-failure in tension, beside the testing temperatures. The elongation-to-failures in tension at room-temperature are obtained to be only 11.5% in the case of grain size of  $50 \mu m$ , but increase to 130% by refining grain size to  $1.5 \mu m$ . Grain refinement is found to be effective to attain a large ductility, in particular, at low strain rate of  $1 \times 10^{-5}/s$ . An increase in testing temperature also causes the enhancement for ductility, irrespective of the grain sizes. For instance, in the meso-grained Mg metal with an average grain size of  $8.6 \mu m$ , this property jumps up from 13% to 53% on an increase in the testing temperature from 273 K to 323 K.

Microstructures before and after tensile tests observed by EBSD in three type grained Mg metals (average grain size of 2.6, 8.6 and  $20 \mu m$ ) are shown in Figs. 6–8. They are observed in the same regions as before

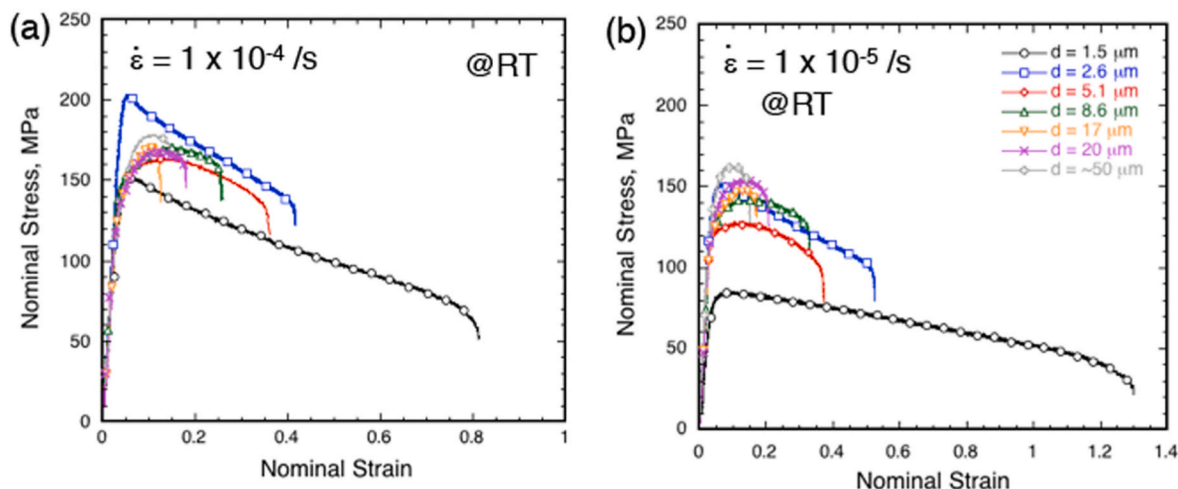


Fig. 3. Nominal stress vs. strain curves at room temperature of the extruded Mg metals (a) at initial strain rate of  $1 \times 10^{-4}/s$  and (b)  $1 \times 10^{-5}/s$ .

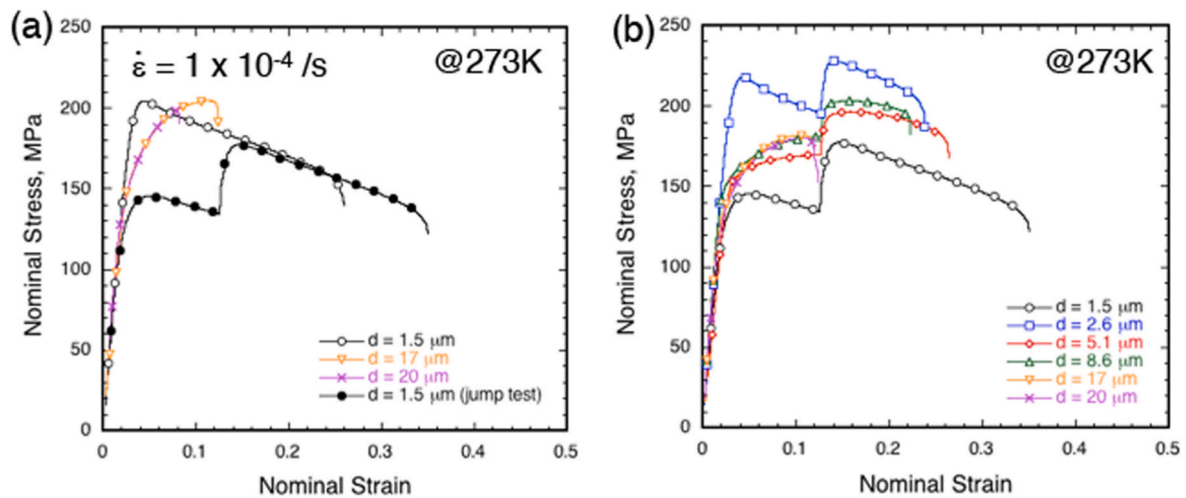


Fig. 4. Nominal stress vs. strain curves at low temperature of 273 K in the extruded Mg metals (a) at initial strain rate of  $1 \times 10^{-4}$ /s and (b) in jump test with strain rate changing from  $1 \times 10^{-5}$  to  $10^{-4}$ /s.

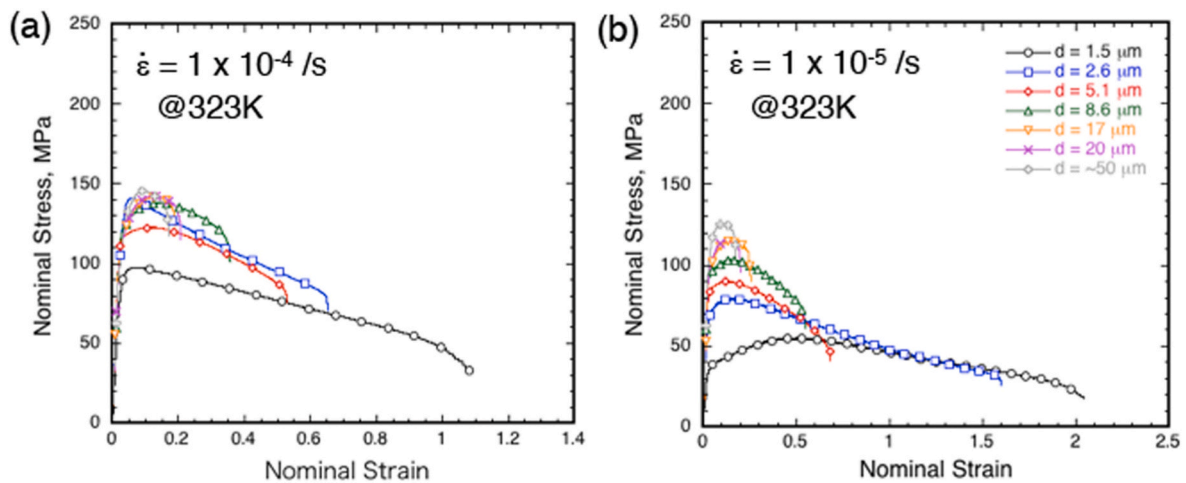


Fig. 5. Nominal stress vs. strain curves at intermediate temperature of 323 K in the extruded Mg metals (a) at initial strain rate of  $1 \times 10^{-4}$ /s and (b)  $1 \times 10^{-5}$ /s.

(Fig. (a)) and after tensile testing (Fig. (b) and (c)) at strain rate of  $1 \times 10^{-5}$ /s in each figure. Figures (a) and (b) show the inverse pole figure images, exhibiting the basal texture as in Fig. 1. Figures (c) are the geometrically necessary dislocation (GND) images adding low- ( $4^\circ \leq \theta < 15^\circ$ ) and high-angle ( $\theta \geq 15^\circ$ ) grain boundaries. On comparison of Figs. (a) and (b), although tensile strain of 0.10 is applied to the specimens, the shape of the grains does not show a prominently noticeable change, irrespective of grain sizes. It is also noted that color gradation changes in certain region, marked by black arrows in Figs. 6(b) and 7(b). This tendency is further readily observed in Figs. 6(c) and 7(c), and corresponding regions consist of a large GND, suggesting the strain (dislocation) accumulation. Such a feature tends to be particularly confirmed in the coarse-grained structures, in particular Figs. 6(c) and 7(c). On the other hand, in Fig. 8(c), it is interesting to notice that most of the grains are unlikely to exhibit these microstructural features, and the vicinity of these grain boundaries as well as grain interiors also do not show a high GND. The grains of less than  $10 \mu\text{m}$  in Figs. 6(c) and 7(c) are also the same features as the fine-grained Mg metal (Fig. 8(c)). Zeng et al. have reported the effect of grain size on deformation mechanism in the grain interior through neutron diffraction, and have shown that the coarse-grains have higher intragranular strains than the fine-grains [18].

In Mg and its alloys, deformation twins preferentially form to make up for a lack of sufficient slip systems at low and room temperatures

during plastic deformation [41]. Fig. 6(c) with line-profile B shows the presence of  $\{1012\}$  type deformation twins marked by the white arrow in the coarse-grains; however, only few fractions are observed in this deformed microstructure. In Figs. 6(c) and 7(c), the line-like contrast features that have a high GND are found to exist in grain interior, marked by black arrows. The misorientation profiles in C and D across this feature are added in these two Fig. (c) on right side. These profiles provide the misorientation angles of point-to-origin. Misorientation angle gradually increases, and then immediately jump up at certain points. The magnitude of such jump-upped misorientation angle is approximately  $3\text{--}4^\circ$ , which suggests sub-grain boundaries in both deformed samples. The results of additional microstructural observation taken by TEM in this region are shown in Fig. 9. STEM image as provided in Fig. 9(a) observed in a (0002) two-beam condition displays line contrasts indicative of basal dislocations with a  $\langle c \rangle$  component, marked by black arrows. Fig. 9(b) shows the same region in the  $\{10\bar{1}0\}$  two-beam condition, and the lower grain is tilted away from a  $\langle 1\bar{2}10 \rangle$  zone axis. In this figure, diffraction patterns of these two tilt conditions are inset, and dashed line denotes approximate orientation of the basal plane. It indicates that dense tangling of dislocations, which can be identified as  $\langle a \rangle$  type basal and non-basal dislocations, marked by white arrows. Diffraction patterns from the two grains indicate that grain boundary misorientation is not large. Although there exists severe

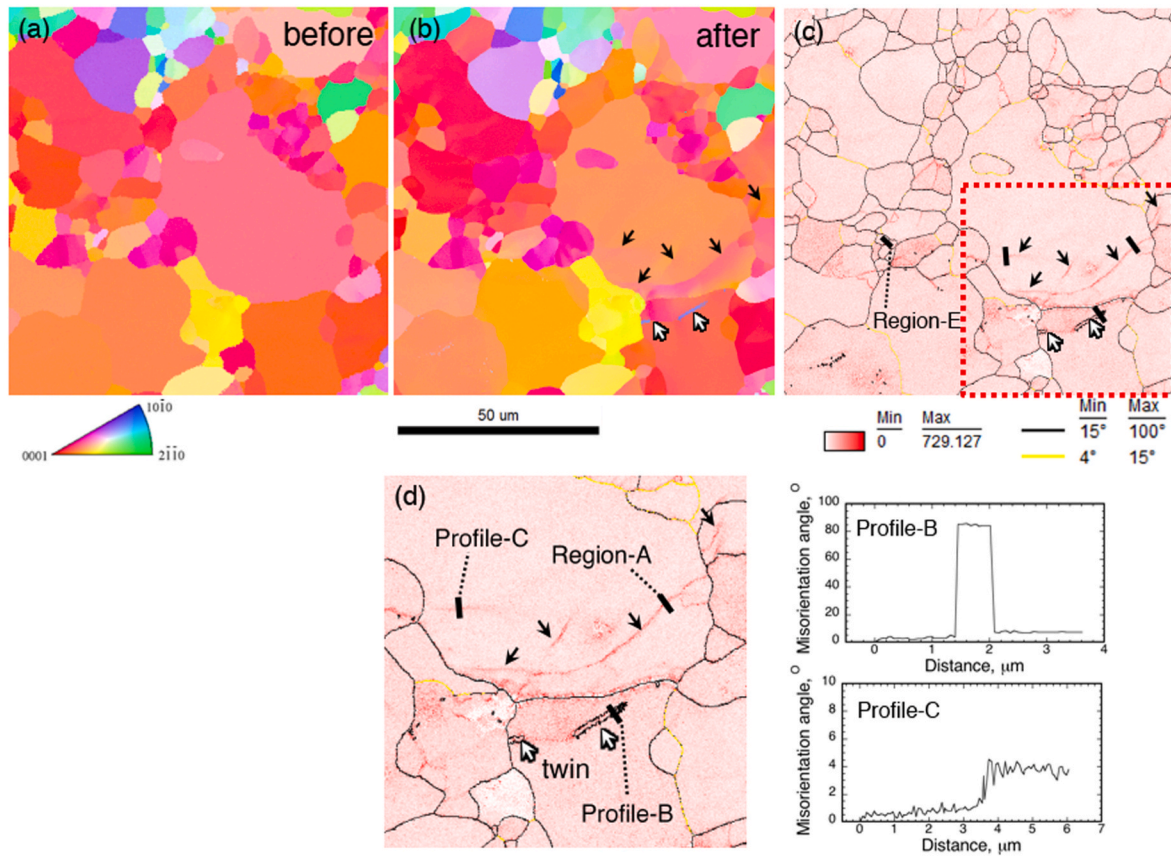


Fig. 6. Microstructures before and after tensile tests observed by EBSD in the Mg metal with grain size of 20  $\mu\text{m}$ : (a), (b) IPF images before and after deformed strain of 0.1, and (c) corresponding GND image in the after state. Figure (d) is the detail of the red dashed area. The analysis of point-to-origin in profiles B and C indicate  $\{10\bar{1}2\}$  twin boundary and sub-grain boundary, respectively, which corresponds to solid white arrows and black arrows. (For interpretation of the references to color in this figure legend, the reader is referred to the Web version of this article.)

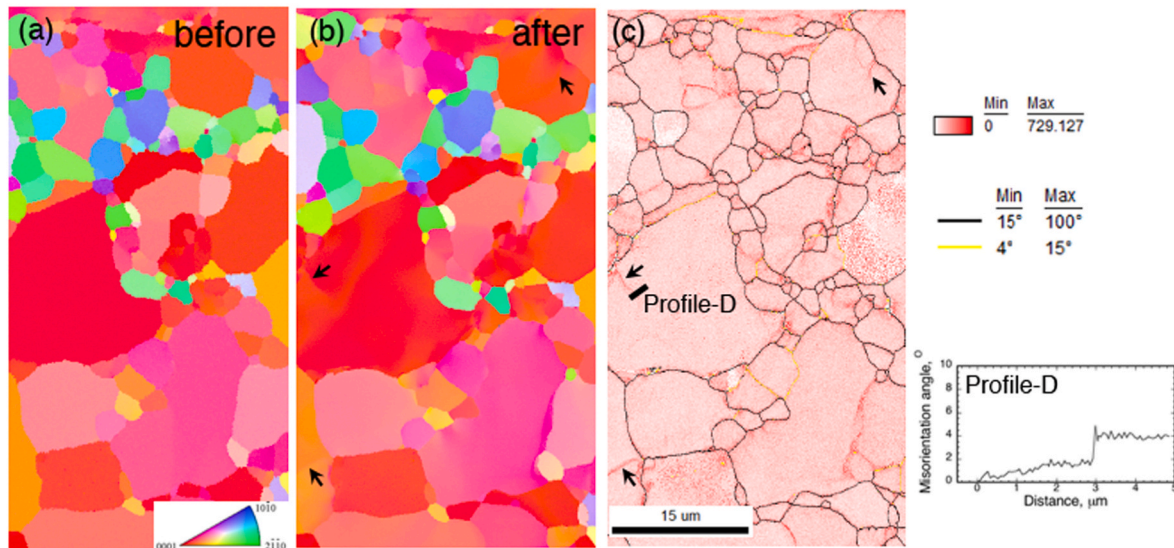


Fig. 7. Microstructures before and after tensile tests observed by EBSD in the Mg metal with grain size of 8.6  $\mu\text{m}$ : (a), (b) IPF images before state and after state on deformed strain of 0.1, and (c) corresponding GND image in the after state. The analysis of point-to-origin in profile D inset Fig. (c), which indicates sub-grain boundary.

strain, some of dislocation are not parallel to the basal plane, which reveals activation of non-basal dislocations. These results indicate progression of sub-grain boundaries via dynamic recrystallization.

Deformed microstructures in the region E, i.e., the vicinity of grain

boundaries, are shown as dark field images in Fig. 10 for (a) (0002) and (b)  $\{10\bar{1}0\}$  two-beam conditions. The origin for these dislocation activities is assumed to be grain boundary compatibility and/or piled up associated with grain boundary sliding; however, by comparison of each

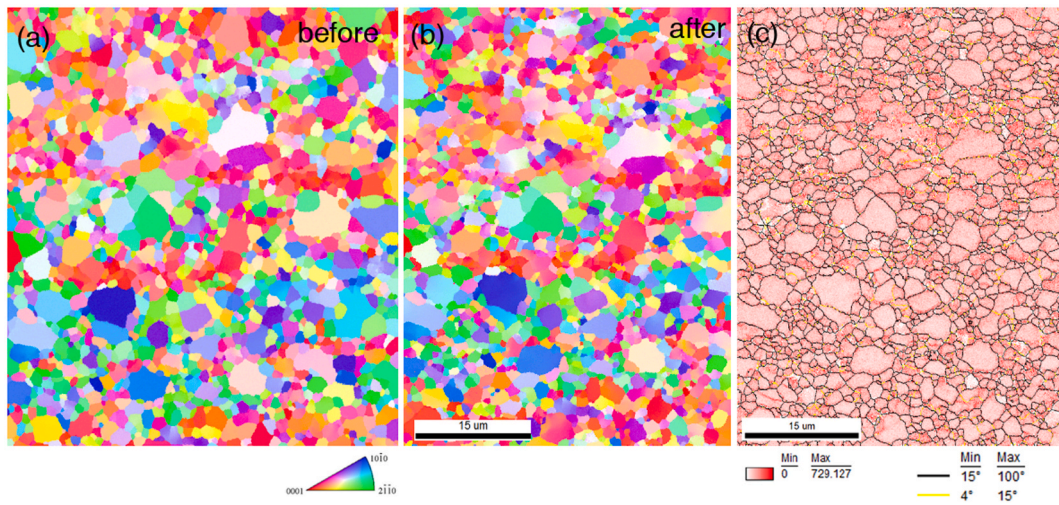


Fig. 8. Microstructures before and after tensile tests observed by EBSD in the Mg metal with grain size of 2.6 μm: (a), (b) IPF images before state and after state on deformed strain of 0.1, and (c) corresponding GND image in the after state.

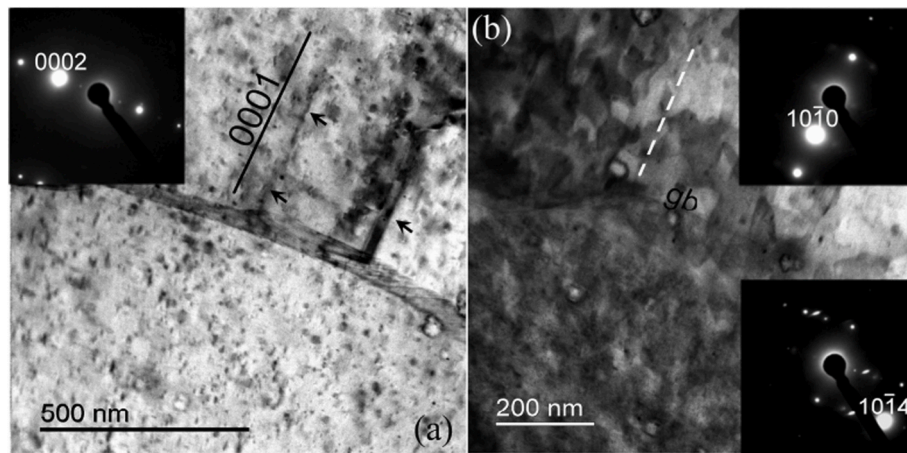


Fig. 9. TEM images from the region A marked in Fig. 6. (a) STEM image of a grain boundary. The upper grain is in a (0002) two-beam diffraction orientation (diffraction pattern from conventional imaging inset), and the black line denotes the orientation of the basal plane. (b) another STEM image in the same region in a different orientation. The upper grain is in a {10 $\bar{1}$ 0} two-beam diffraction orientation (diffraction patterns inset).

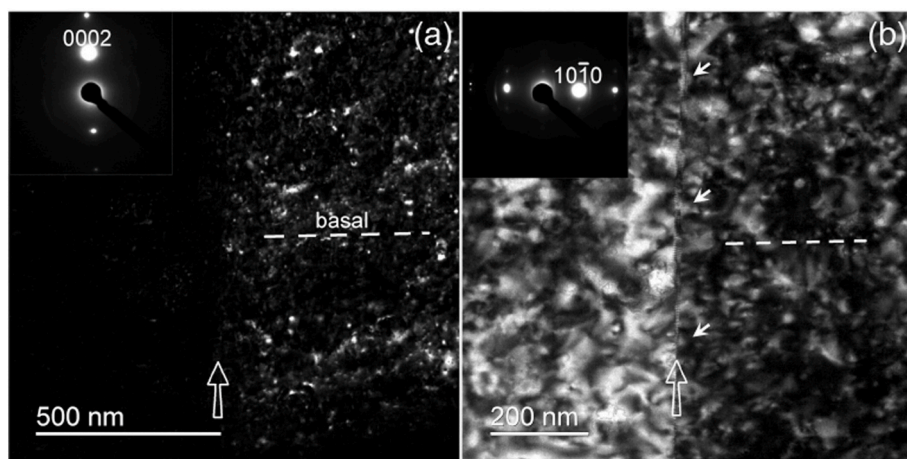


Fig. 10. TEM images from the region E marked in Fig. 6 taken by (a) (0002) and (b) {10 $\bar{1}$ 0} two-beam diffraction orientations. where open arrows indicate grain boundary and white arrows are dislocations at grain boundary.

image (and the  $g \cdot b$  criterion), it is found the activation of non-basal dislocations at grain boundaries, marked by arrows.

Fig. 11 shows the surface and deformed microstructural observations of the specimens (fine- and meso-grained Mg metals) taken by SEM and EBSD. In all the images, tensile direction is parallel to the horizontal direction. In Fig. 11(a) and (b), surface features are found to be changed by grain size; high amounts of cotton-like features, marked by white arrows, exist in the fine-grained Mg metal. This feature, i.e., trace of grain boundary sliding, is well-observed in the deformed specimens that exhibit extremely large elongation-to-failure, recognized as superplasticity [42]. In contrast, the fraction of such a trace reduces in the meso-grained Mg metal, as shown in Fig. 11(b). Fig. 11(c) is the inverse pole figure image from the vicinity of fracture in meso-grained Mg metal. The  $\{10\bar{1}2\}$  type deformation twins, marked by white arrows, are confirmed to form, as in the deformed specimens with tensile strain of 0.10 (Fig. 6); while, the area fraction is not high even in the vicinity of the fracture. It is also noted that some of the grains show color gradation. Typical line-profile in the region F is inset at the right-bottom side in the image; misorientation angle profile shows a gradual rather than an immediate increase at a certain point. The profile feature of misorientation angle in Fig. 11(c) is different from those in Figs. 6 and 7. Our previous TEM study reveals that this noticeable color change has a close relation to cross- and/or multiple-slip, owing to the activity of non-basal dislocation slip [43].

#### 4. Discussion

The mechanical properties of Mg and its alloys are strongly related to a strong basal texture, owing to their HCP structures. Several studies have reported that the elongation-to-failure in tension as well as yield strength changes with the basal plane distribution [44–46]. It is well-recognized that the equal-channel-angular extruded Mg alloy exhibits twice larger ductility but lower yield strength as compared with those of extruded alloy in quasi-static strain rate tensile tests [2]. This is due to this specific alloy having the basal plane tilted to  $45^\circ$  to the tensile/wrought-processing direction, namely, a high Schmid factor of  $< 11\bar{2}0 \rangle(0002)$ . The Schmid factor of the basal plane is obtained to be

0.34 vs. 0.18 for the ECAE-ed and extruded alloys, respectively [47]. The microstructural observations (Fig. 1) show that the present extruded Mg metals show a basal texture. In Table 1, Schmid factors for these Mg metals are 0.16–0.22, which is close to the previous reported value of 0.18 in extruded Mg alloy; hence, the contribution of texture (basal plane distribution) to mechanical properties are almost similar. Misorientation angle distribution is also known to be the other influential factors on deformation behavior, as well as the mechanical properties and diffusivities. Grain boundary characteristic, i.e., grain boundary energy, have a close relation to the magnitude of grain boundary sliding; grain boundaries with a low (or high) grain boundary energy suppress (or enhance) grain boundary sliding, respectively [48–50]. In other words, low-angle and coincident site lattice grain boundaries have a lower contribution of grain boundary sliding on deformation, because such grain boundaries consist of a lower grain boundary energy than that of general grain boundaries, such as high-angle grain boundaries [51,52]. Similar to the deformation behavior, Mg alloys having high volume fraction of low-angle grain boundaries ( $\theta < 15^\circ$ ) are pointed out to have superior toughness (high crack-propagation resistance), compared with those of the alloys having a low volume fraction of these specific boundaries [34]. In addition, grain boundary structures affect diffusion rate [53–57]; nevertheless, irrespective of extrusion temperatures, the present Mg metals have similar average misorientation angles and volume fractions of low-angle grain boundaries, as listed in Table 1. Thus, these two major influential factors can be ignored; hereafter, we entirely focus on the argument of the grain size effect.

##### 4.1. Deformation mechanism

The dependence of strain rate on flow stress is represented by the strain rate sensitivity, which is the so-called  $m$ -value, and is a well-known method to consider deformation mechanism. The  $m$ -value in room-temperature tensile tests fell between 0.026 and 0.219 for all extruded Mg studied here (average grain sizes of  $1.5 \mu\text{m}$  to  $\sim 50 \mu\text{m}$ ), as listed in Table 1. The strain rate sensitivity is found to increase with grain refinement. In previous studies, fine-grained Mg metals with average grain sizes of  $0.65 \mu\text{m}$  and  $1.2 \mu\text{m}$  indicate large  $m$ -values of

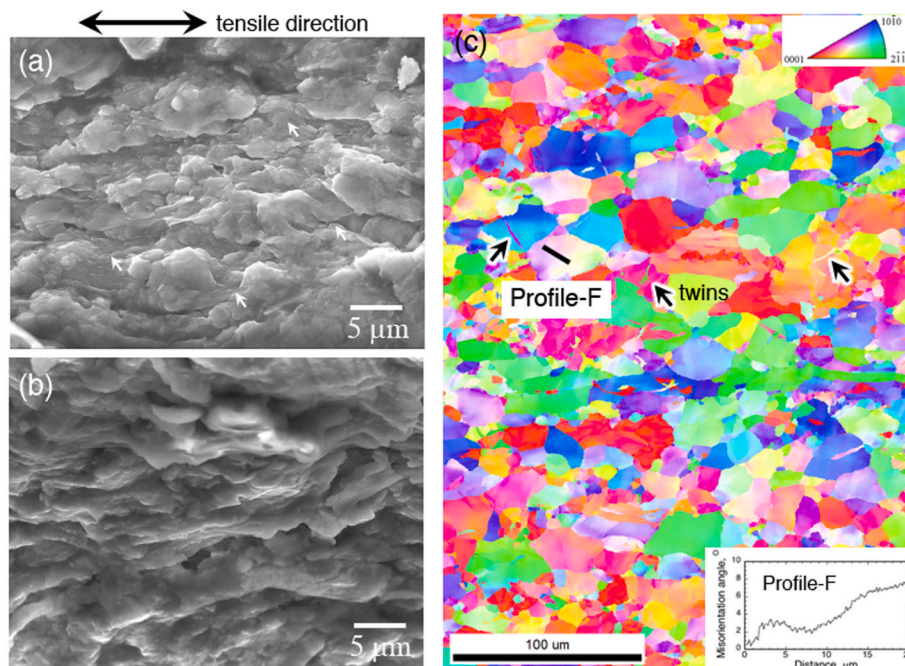


Fig. 11. Surface and internal microstructural observations of the fractured specimens taken by SEM and EBSD: (a) fine-grained Mg metal with grain size of  $2.6 \mu\text{m}$  and (b), (c) meso-grained Mg metal with grain size of  $17.6 \mu\text{m}$  where black arrows in Fig. (c) indicate  $\{10\bar{1}2\}$ -type deformation twins.

0.14 at quasi-static strain rates [21] and 0.23 at low strain rates [20]. While the  $m$ -values in Table 1 are obtained at low strain rate regimes, the present Mg metals clearly show lower  $m$ -values than those reported values, because of the coarser-grain size. The  $m$ -values obtained from the other testing temperatures of 273 K and 323 K are also provided in Table 1. The  $m$ -value tends to be higher with an increase in testing temperature; for instance, extruded Mg with an average grain size of 2.6  $\mu\text{m}$  has the  $m$ -values of 0.067 at 273 K and 0.232 at 323 K.

As compared to the general trend regarding dominant deformation behavior, when deformation twins are the major deformation mode, the  $m$ -value is almost zero, owing to the weak thermally activated process [41,58,59]. However, all the extruded Mg metals are unlikely to show such a small value, even at the temperature of 273 K. In Figs. 6 and 11 (c),  $\{10\bar{1}2\}$  type deformation twins are formed in some grains at an applied strain of 0.1 and even after rupture, but such deformed features display only a small fraction of the total. When twinning particularly contribute to deformation, e.g., during compressive tests, the area fraction of these twins is large, more than 0.10 [60,61]. Apart from the deformation twins, in the case of  $m$ -value of  $\sim 0.01$ – $0.05$ , dislocation slip is a dominant deformation mechanism [42]. This is well applicable to the present meso- and coarse-grained Mg metals at low and room temperatures. Alternative to a few traces of grain boundary sliding, some of grains show a color change mapping that is associated with a gradual increase in misorientation angle. These features imply dislocation slips as dominant deformation mechanism. On the other hand, fine-grained Mg metals exhibit high  $m$ -values of more than 0.1 even at 273 K, and the  $m$ -value in all the Mg metals increase above 0.05 with an increase in testing temperature to 323 K. These  $m$ -values suggest that different deformation mechanisms are activated in fine-grained Mg metals in temperature range of 237 K–323 K and in most of the Mg metals at intermediate temperatures. It is noted that several studies as well as the present result (Fig. 11(a)) show traces of grain boundary sliding in room temperature deformed Mg and its alloys [16,21,24]. When grain boundary sliding is the rate-controlling deformation mechanism, i.e., superplastic behavior, the  $m$ -values generally lie between 0.3 and 0.5 [42,62]. The results (in Table 1) show that the fine-grained Mg metals do not exhibit such a large  $m$ -value; thus, grain boundary sliding is assumed to partially contribute to deformation in the fine-grained Mg metals.

The variation of elongation-to-failure in tension and  $m$ -value as a function of average grain size are shown in Fig. 12. It is noted that the elongation-to-failure in tension is measured by the butt match method. This figure includes the previously reported results of Mg metals [20], and every value of reported elongation-to-failure in tension at the strain rate of  $1 \times 10^{-5}/\text{s}$  is cited. The elongation-to-failure in tension in the grain size of  $\sim 20 \mu\text{m}$  is approximately 20–30%, which is of similar value to that of common Mg alloys; however, this property significantly enhances with grain refinement and exhibits more than 100%, when the grain sizes refine to approximately 2–3  $\mu\text{m}$ . Similar to the correlation between grain size and ductility, in Fig. 12(b), the  $m$ -values are found to depend on grain size, irrespective of testing temperatures. As mentioned above, the strain rate sensitivity shows low value at low temperature (273 K), but increases with testing temperatures. A comparison with Fig. 12(a) shows that the influence of grain size on the  $m$ -value has the same tendency. These results suggest that ductility is closely related to the  $m$ -value, i.e., obtaining a large ductility at the condition of showing a high  $m$ -value of  $>0.05$ .

It is noticed in Fig. 12 that grain refinement impact from 5  $\mu\text{m}$  to 1  $\mu\text{m}$  has a large magnitude in increase of  $m$ -value (and elongation-to-failure in tension), compared with that from 50  $\mu\text{m}$  to 10  $\mu\text{m}$ . Particularly, when the average grain size is coarser than approximately 3–5  $\mu\text{m}$ , the ductility and  $m$ -value significantly reduce; in the other words, this grain size is the transition point of change in the deformation mechanism. Grain boundary compatibility is reported to operate in the vicinity of grain boundaries in polycrystalline Mg alloy during plastic deformation [1]. This concept has been developed for metallic bicrystals;

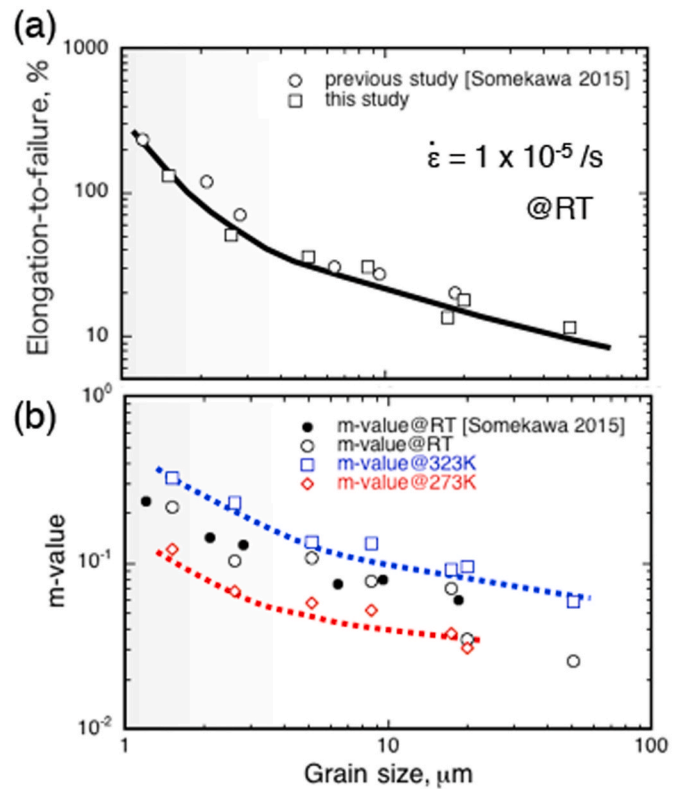


Fig. 12. The variation of (a) elongation-to-failure in tension and (b)  $m$ -value as a function of average grain size in the Mg metals.

when a large stress field is operated at grain boundaries, different type of slip systems are activated to continue plastic deformation [63–65]. The influential distance for such compatibility to occur is estimated to be the distance in several micrometers. Deformed microstructural observations on the Mg alloys have pointed out the non-basal dislocation activities owing to compatibility operation in the whole grains, when the grain size is 10  $\mu\text{m}$  [66]. Room-temperature nanoindentation creep tests have revealed that the strain rate sensitivity is  $\sim 0.5$  at grain boundaries, but is down to  $\sim 0.1$  far from grain boundaries [15]. Despite the empirical result, the transitional grain boundary distance, at which grain boundary sliding occurs or is suppressed, is approximately 5  $\mu\text{m}$ . This localized creep behavior suggests a high occurrence of grain boundary sliding at grain boundaries. As compared with these previous studies, the present transitional grain size of 3–5  $\mu\text{m}$  is interestingly in a similar range, in Fig. 12. Thus, one of the reasons for a significant improvement in ductility and strain rate sensitivity results from an enhancement of grain boundary plasticity, such as non-basal dislocations and grain boundary sliding, in the whole grains.

#### 4.2. Accommodation mechanism

In superplastic flow, two types of accommodation processes for grain boundary sliding have been well-recognized to be diffusional flow [67] and diffusion-controlled dislocation slip [32,33] for several decades. In recent studies, the latter model of diffusion-controlled dislocation slip is adequate to describe conventional superplastic flow, i.e., under the conditions of high temperatures and low strain rates. Deformed microstructural observations have certified the activation of dislocation slip in superplastic Mg alloys [68], and these dislocation slips are accommodated by lattice diffusion in coarse-grains at high temperatures ( $>0.7T_m$ ; where  $T_m$  is the melting point) and grain boundary diffusion in fine-grains at low temperatures ( $<0.7T_m$ ) [31]. Beside these results, room-temperature deformed Mg metals which exhibit a huge tensile

elongation associated with grain boundary sliding have also been reported to show a lot of dislocation slip traces consisting of the non-basal types in the matrix [20,21]. In addition, high densities of dislocations are activated even on the magnitude of an applied strain of 0.10, as provided in Fig. 10. Therefore, an accommodation process for this unique room-temperature grain boundary sliding is necessary to continue plastic deformation and to attain a large ductility, as in the common superplastic flow at high temperatures. Hereafter, it will be considered what is related to and dominated in this slip accommodation process.

An understanding and measurement of activation energy are useful to further take into account for the accommodation process, from a thermomechanical viewpoint. In plastic deformation at low strain rate regimes, the relationship between strain rate and flow stress normalized by shear modulus,  $G$ , is generally expressed as;

$$\dot{\epsilon} = A(\sigma/G)^n \times D_0 \exp(-Q/RT) \quad (1)$$

where  $A$  is a constant,  $n$  is the stress exponent ( $= 1/m$ ),  $D_0$  is the diffusion coefficient,  $Q$  is the activation energy for diffusion,  $R$  is the gas constant and  $T$  is the temperature. By using the tensile test results within three temperature ranges, typical examples for correlation between the normalized stress,  $(\sigma/G)$ , and the reciprocal temperature are shown in Fig. 13. The slope in this figure is the activation energy, which are calculated to be 79.0 kJ/mol and 30.9 kJ/mol for the extruded Mg metals having average grain sizes of 1.5  $\mu\text{m}$  and 17.2  $\mu\text{m}$ , respectively. The activation energies in the present study are summarized in Table 1. These activation energies are found to depend on grain size; this value becomes higher with grain refinement. The fine-grained Mg metals have the activation energies in the range of 65–80 kJ/mol, which are close to that of grain boundary diffusion of  $Q_{\text{gb}} = 92$  kJ/mol [4]. Figueiredo et al. have reported that the activation energy of fine-grained Mg metal is 75 kJ/mol in compressive tests at the temperatures of 296 K–373 K [19]. On the other hand, this activation energy reduces with grain coarsening and tends to be a constant of  $\sim 30$  kJ/mol. It is noted that the correlation between activation energy and grain size is similar to that of the effect of grain size on strain rate sensitivity and elongation-to-failure in tension, as shown in Fig. 12.

Grain boundary diffusion rate at room-temperature is calculated to be 0.67 nm/s ( $= D_{0\text{gb}} \times \exp(-Q_{\text{gb}}/RT)$ , where  $D_{0\text{gb}} = 7.8 \times 10^{-3}$  m<sup>2</sup>/s [4]). The diffusion distance per 1 s corresponds to several atom orders; while, it needs to be drawn to attention that this influential region or distance is at least two or three times larger than that of the other metals, such as Cu and Ni metals [4], in which the inverse Hall-Petch behavior

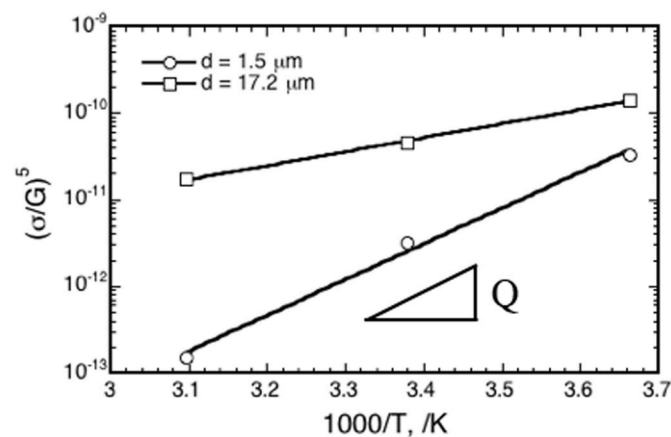


Fig. 13. Typical examples for correlation between the normalized stress,  $(\sigma/G)$ , and the reciprocal temperature. This equation (1) can be re-written to  $(\sigma/G)^n = (\dot{\epsilon}/A) \times (1/D_0) \times \exp(Q/RT)$ . When the flow stress,  $\sigma$ , would be used from the strain rate,  $\dot{\epsilon}$ , of  $1 \times 10^{-5}$ /s, the slope in this relation corresponds to the activation energy of  $Q$ .

occurs. Since diffusion rates become fast with an increase in temperature, grain boundary diffusion rate at room-temperature is much slower than that at common conditions for superplastic flow, e.g.,  $D_{\text{gb}} = 5.7$   $\mu\text{m}/\text{s}$  at 573 K. However, such a small influential region or distance via grain boundary diffusion is enough to diffuse each atom as well as vacancies, because dislocations also consist of atomistic order, which is very similar in size associated with grain boundary diffusion. This result shows that, in fine-grained Mg metals, diffusion process through grain boundary diffusion has a possibility to play an important role in removing and disappearing of the piled-up dislocations at grain boundary. This is supported by Figs. 6–8 which shows that the vicinity of grain boundaries is unlikely to show many residual strains for fine-grained structures. Several results also reveal that diffusion rate increases with grain refinement, due to an increase in volume fraction of grain boundaries besides triple points of grain boundary, as in case of previous reports [69,70].

On the other hand, this tendency implies that contribution of grain boundary diffusion becomes small with increasing grain sizes (grain boundary density); as a result of low activation energies in the meso- and coarse-grained Mg metals. In the meso-grained Mg alloy (AZ31 alloy) with an average grain size of 20  $\mu\text{m}$ , the activation energy is roughly estimated to be  $\sim 20$  kJ/mol [16]. The further lower activation in the Mg alloy is assumed to be the alloying of aluminum, which affect diffusivity and accommodation process. In our previous study, Mg–Al binary alloy shows a higher onset temperature for grain boundary sliding to that of Mg metals [43]; however, the tendency for a lower activation energy in the meso-grained structures is in agreement with the present tendency for grain size dependence. In this paper, slip-induced grain boundary sliding occurs at such a low activation energy [16]. This slip-induced grain boundary sliding is developed in the HCP metals, according to grain boundary behavior [71,72]. Matsunaga et al. have reported using various Zn metals (with grain size of 20–500  $\mu\text{m}$ ) that the accumulated dislocations at grain boundaries disappeared by not diffusional flow but lattice rotation [73]. The activation energy is obtained to be  $\sim 20$  kJ/mol in this deformation mechanism at “quite low” strain rates of  $< 1 \times 10^{-7}$ /s; however, there are remarkable differences in strain rates. In addition, the physical and material characteristic affecting plastic flow vary; for instance, the Zn metal has (i) a lower difference of CRSS between the basal and non-basal plane [74] and (ii) a higher  $c/a$  ratio, compared with those in Mg metal [75]. It is interesting to notice that the lattice rotation owing to lattice dislocation is also unlikely to be considered in the present Mg metals. Thus, one of the reasons for decrease in activation energy is simply associated with low volume fraction of grain boundaries having a high diffusion rate.

Deformed microstructures in Figs. 6 and 7 additionally support this point; grains consisting of meso- and coarse-sizes have larger GND as compared to those of fine-sizes. Intragranular deformation readily occurs in these grains, due to a lack of sufficient (grain boundary) diffusional flow into grain interior. These results also show that the residual dislocations, which are unlikely to disappear by diffusional flow, form sub-grain boundaries. Grain boundary sliding induced recrystallization is observed in several metallic materials as the condition for superplasticity to occur [76,77]. Masuda et al. have pointed out that this recrystallization behavior has a close relation to the accommodation process for dislocation slip [78,79]. In the present case, although the contribution of grain boundary sliding to deformation is not large in the meso- and coarse-grains, recrystallization owing to grain boundary sliding is an alternative accommodation mode for insufficiently dominant diffusional flow process. Simple illustrations for the effect of grain size on room-temperature grain boundary sliding are provided in Fig. 14. In the fine-grained Mg metals, inducing dislocations owing to grain boundary sliding slip on the basal (and non-basal) planes to relax the stress concentration at triple points of grain boundaries, and then these dislocations are piled up on opposite grain boundaries. To prevent early rupture, these piled up dislocations vanish and/or eliminate via diffusion process at grain boundaries, as shown in Fig. 14(a). The same

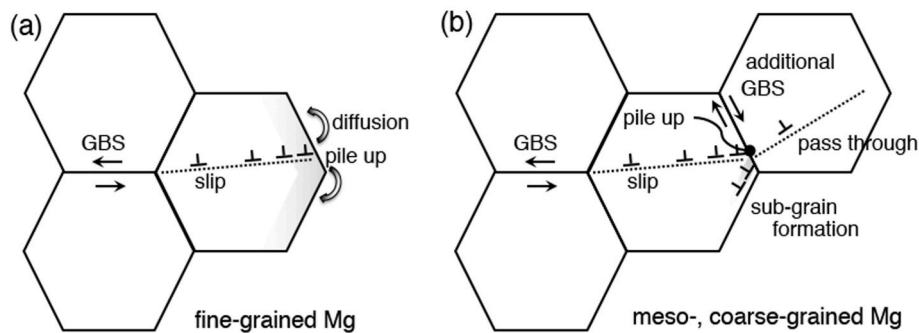


Fig. 14. Illustration of slip accommodation process at room-temperature grain boundary sliding (a) in the fine-grained Mg and (b) meso- and coarse-grained Mg metals.

behavior would take place in the meso- and coarse-grained Mg metals; however, the contribution of diffusion process to accommodation is limited because of a decrease in grain boundary density. Some of dislocations cross grain boundaries, as in the case of general plastic deformation in metallic materials. In contrast, residual dislocations, i.e., dislocations that do not disappear through diffusion process, become sites for sub-grain boundaries, and others play a role in the occurrence of additional slip-induced grain boundary sliding, as provided in Fig. 14 (b).

## 5. Conclusions

In order to clarify the role of grain boundary plasticity on plastic deformation at ambient temperatures in bulk Mg metals, deformation mechanism as well as deformed microstructures were investigated using several extruded Mg metals with different grain sizes. The following results were obtained.

- (1) Uniaxial tensile tests show that the strain rate sensitivity and elongation-to-failure increase with grain refinement, regardless of the testing temperatures. Fine-grained Mg metal with grain size of  $\sim 1 \mu\text{m}$  has the  $m$ -value of 0.2, which is lower than that of common superplastic metallic materials. However, the activation energy becomes high value from 30 to 80 kJ/mol, corresponding to grain boundary diffusion in Mg metal.
- (2) Deformed microstructural observations after tensile tests prove that some of grains have accumulation of strains at grain boundaries; whereas, such fraction tends to decrease with grain refinement associated with an increase in grain boundary fractions. In the meso- and coarse-grains, intergranular deformation mode, such as dislocation slip, is dominant and sub-grain boundaries are formed to make up for the lack of grain boundary plasticity.
- (3) Accommodation process for dislocation slip during room-temperature grain boundary sliding has a close relationship with the grain size in the Mg metals. The contribution of diffusion process is large in the fine-grained Mg metals, but decreases with grain coarsening (lower grain boundary density).

## CRedit authorship contribution statement

**Hidetoshi Somekawa:** Conceptualization, Investigation, Data curation, Validation, Writing – original draft, review & editing, Project administration, Funding acquisition. **Masato Wakeda:** Data curation, Validation, Writing – review & editing. **Alok Singh:** Investigation, Data curation, Validation, Writing – review & editing.

## Declaration of competing interest

The authors declare that they have no known competing financial

interests or personal relationships that could have appeared to influence the work reported in this paper.

## Acknowledgement

The authors are grateful to Dr. T. Hiroto, Ms. R. Komatsu and Ms. M. Sanbu (National Institute for Materials Science) for their technical help. This work was partially supported by the JSPS Grant-in-Aid in No. 19K05068.

## References

- [1] J. Koike, K. Kobayashi, T. Mukai, H. Watanabe, M. Suzuki, K. Maruyama, K. Higashi, The activity of non-basal slip systems and dynamic recovery at room temperature in fine-grained AZ31B magnesium alloys, *Acta Mater.* 51 (2003) 2055–2065.
- [2] T. Mukai, M. Yamanoi, H. Watanabe, K. Higashi, Ductility enhancement in AZ31 magnesium alloy by controlling its grain structure, *Scripta Mater.* 45 (2001) 89–94.
- [3] F. Wang, S.R. Agnew, Dislocation transmutation by tension twinning in magnesium alloy AZ31, *Int. J. Plast.* 81 (2016) 63–86.
- [4] H.J. Frost, J.F. Ashby, *Deformation-mechanism Map*, Pergamon Press, Oxford, 1982.
- [5] A. Al-Zubaydi, A.P. Zhilyaev, S.C. Wang, P.A.S. Reed, Superplastic behavior of AZ91 magnesium alloy processed by high-pressure torsion, *Mater. Sci. Eng. A637* (2015) 1–11.
- [6] E. Mostaed, A. Fabrizio, D. Dellasega, F. Bonollo, M. Vedani, Microstructure, mechanical behavior and low temperature superplasticity of ECAP processed ZM21 Mg alloy, *J. Alloys Compd.* 638 (2015) 267–276.
- [7] H. Matsunoshita, K. Edalati, M. Furui, Z. Horita, Ultrafine-grained magnesium-lithium alloy processed by high-pressure torsion: low-temperature superplasticity and potential for hydroforming, *Mater. Sci. Eng. A640* (2015) 443–448.
- [8] T.J. Lee, W.J. Kim, Successful transition from low-temperature superplasticity to high-strain-rate superplasticity with increasing temperature in an ultrafine-grained Mg-Y-Zn-Zr alloy, *J. Alloys Compd.* 817 (2020), 153298.
- [9] V.N. Chuvildev, T.G. Nieh, Y.M. Gryaznov, A.N. Sysoev, V.I. Kopylov, Low-temperature superplasticity and internal friction in microcrystalline Mg alloys processed by ECAP, *Scripta Mater.* 50 (2004) 861–865.
- [10] H. Watanabe, T. Mukai, T.G. Nieh, K. Higashi, Low temperature superplasticity in a magnesium-based composite, *Scripta Mater.* 42 (2000) 249–255.
- [11] M. Mabuchi, K. Ameyama, H. Iwasaki, K. Higashi, Low temperature superplasticity of AZ91 magnesium alloy with non-equilibrium grain boundaries, *Acta Mater.* 47 (1999) 2047–2057.
- [12] K. Matsubara, Y. Miyahara, Z. Horita, T.G. Langdon, Developing superplasticity in a magnesium alloy through a combination of extrusion and ECAP, *Acta Mater.* 51 (2003) 3073–3084.
- [13] H. Watanabe, T. Mukai, K. Ishikawa, M. Mabuchi, K. Higashi, Realization of high-strain-rate superplasticity at low temperatures in a Mg-Zn-Zr alloy, *Mater. Sci. Eng. A307* (2001) 119–128.
- [14] C.L. Wang, T. Mukai, T.G. Nieh, Room temperature creep of fine-grained pure Mg: a direction comparison between nanoindentation and uniaxial tension, *J. Mater. Res.* 24 (2009) 1615–1618.
- [15] H. Somekawa, T. Mukai, Nanoindentation creep behavior of grain boundary in pure magnesium, *Phil. Mag. Lett.* 90 (2010) 883–890.
- [16] J. Koike, R. Ohyama, T. Kobayashi, M. Suzuki, K. Maruyama, Grain boundary sliding in AZ31 magnesium alloys at room temperature to 523 K, *Mater. Trans.* 44 (2003) 445–451.
- [17] Z. Zeng, J.F. Nie, S.W. Xu, C.H.J. Davies, N. Birbilis, Super-formable pure magnesium at room temperature, *Nat. Commun.* 8 (2017) 972.
- [18] Z. Zeng, M. Zhou, P. Lynch, F. Momprou, Q. Gu, M. Esmaily, Y. Yan, Y. Qiu, S. Xu, H. Fujii, C. Davies, J.F. Nie, N. Birbilis, Deformation modes during room temperature tension of fine-grained pure magnesium, *Acta Mater.* 206 (2021), 116648.

- [19] R.B. Figueiredo, S. Sabbaghianrad, A. Giwa, J.R. Greer, T.G. Langdon, Evidence for exceptional low temperature ductility in polycrystalline magnesium processed by severe plastic deformation, *Acta Mater.* 122 (2017) 322–331.
- [20] H. Somekawa, T. Mukai, Hall-Petch breakdown in fine-grained pure magnesium at low strain rates, *Metall. Mater. Trans.* 46A (2015) 894–902.
- [21] R. Zheng, J.P. Du, S. Gao, H. Somekawa, S. Ogata, N. Tsuji, Transition of dominant deformation mode in bulk polycrystalline pure Mg by ultra-grain refinement down to sub-micrometer, *Acta Mater.* 198 (2020) 35–46.
- [22] H. Somekawa, A. Singh, Superior room temperature ductility of magnesium dilute binary alloy via grain boundary sliding, *Scripta Mater.* 150 (2018) 26–30.
- [23] H. Somekawa, A. Singh, T. Mukai, T. Inoue, Effect of alloying elements on room temperature tensile ductility in magnesium alloys, *Phil. Mag.* 96 (2016) 2671–2685.
- [24] H. Somekawa, Effect of alloying elements on fracture toughness and ductility in magnesium binary alloys, A review, *Mater. Trans.* 61 (2020) 1–13.
- [25] F. Momprou, M. Legros, A. Boe, M. Coulombier, J.P. Raskin, T. Pardoen, Inter- and intragranular plasticity mechanisms in ultrafine-grained Al thin films; an in situ TEM study, *Acta Mater.* 61 (2013) 205–216.
- [26] E. Alabort, P. Kontis, D. Barba, K. Dragnevski, R.C. Reed, On the mechanisms of superplasticity in Ti-6Al-4V, *Acta Mater.* 105 (2016) 449–463.
- [27] D.H. Bae, A. Ghosh, Cavity formation and early growth in a superplastic Al-Mg alloy, *Acta Mater.* 50 (2002) 511–523.
- [28] F. Giuntoli, A.V. Brovarone, L. Menegon, Feedback between high-pressure genesis of abiogenic methane and strain localization in subducted carbonate rocks, *Sci. Rep.* 10 (2020) 9848.
- [29] C. Xu, M. Furukawa, Z. Horita, T.G. Langdon, Using ECAP to achieve grain refinement, precipitate fragmentation and high strain rate superplasticity in a spraycast aluminum alloy, *Acta Mater.* 51 (2003) 6139–6149.
- [30] H. Somekawa, D.A. Basha, A. Singh, Room temperature grain boundary sliding behavior of fine-grained Mg-Mn alloys, *Mater. Sci. Eng. A730* (2018) 355–362.
- [31] H. Watanabe, T. Mukai, M. Kohzu, S. Tanabe, K. Higashi, Effect of temperature and grain size on the dominant diffusion process for superplastic flow in an AZ61 magnesium alloy, *Acta Mater.* 47 (1999) 3753–3758.
- [32] A. Ball, M.M. Hutchinson, Superplasticity in the aluminum-zinc eutectoid, *Mater. Sci. J.* 3 (1969) 1–7.
- [33] A.K. Mukherjee, The rate controlling mechanism in superplasticity, *Mater. Sci. Eng. A8* (1971) 83–89.
- [34] H. Somekawa, A. Singh, T. Inoue, Enhancement of fracture toughness by grain boundary control in magnesium binary alloys, *Mater. Sci. Eng. A612* (2014) 172–178.
- [35] C.A. Schuh, T.G. Nieh, H. Iwasaki, The effect of solid solution W additions on the mechanical properties of nanocrystalline Ni, *Acta Mater.* 51 (2003) 431–443.
- [36] J. Schiotz, F.D. Di Tolla, K.W. Jacobsen, Softening of nanocrystalline metals at very small grains, *Nature* 391 (1998) 561–563.
- [37] J. Schiotz, K.W. Jacobsen, A maximum in the strength of nanocrystalline copper, *Science* 301 (2003) 1357–1359.
- [38] M.A. Meyers, A. Mishra, D.J. Benson, Mechanical properties of nanocrystalline materials, *Prog. Mater. Sci.* 51 (2006) 427–556.
- [39] A.M. Elshierik, U. Erb, Synthesis of bulk nanocrystalline nickel by pulsed electrodeposition, *J. Mater. Sci.* 30 (1995) 5743–5749.
- [40] V.Y. Gertsman, M. Hoffmann, H. Gleiter, R. Birringer, The study of grain size dependence of yield stress of copper for a wide grain size range, *Acta Metall. Mater.* 42 (1994) 3539–3544.
- [41] J.W. Christian, S. Mahajan, Deformation twinning, *Prog. Mater. Sci.* 39 (1995) 1–157.
- [42] J. Wadsworth, O.D. Sherby, Superplasticity recent advances and future directions, *Prog. Mater. Sci.* 33 (1989) 169–221.
- [43] H. Somekawa, M. Yamaguchi, Y. Osawa, A. Singh, M. Itakura, T. Tsuru, T. Mukai, Material design for magnesium alloys with high deformability, *Phil. Mag.* 95 (2015) 869–885.
- [44] B.C. Suh, M.S. Shim, K.S. Shin, N.J. Kim, Current issues in magnesium sheet alloys; where do we go from here? *Scripta Mater.* 84–85 (2014) 1–6.
- [45] Z. Zeng, N. Stanford, C.H.J. Davies, J.F. Nie, N. Birbilis, Magnesium extruded alloys; a review of developments and properties, *Int. Mater. Rev.* 64 (2019) 27–62.
- [46] J.F. Nie, K.S. Shin, Z.R. Zeng, Microstructure, deformation, and property of wrought magnesium alloys, *Metal. Mater. Trans.* A51 (2020) 6045–6109.
- [47] H. Somekawa, H.S. Kim, A. Singh, T. Mukai, Fracture toughness in direct extruded Mg-Al-Zn alloys, *J. Mater. Res.* 22 (2007) 2598–2607.
- [48] R.Z. Valiev, T.G. Langdon, Principles of equal-channel angular pressing as a processing tool for grain refinement, *Prog. Mater. Sci.* 51 (2006) 881–981.
- [49] H. Kokawa, T. Watanabe, S. Karashima, Sliding behavior and dislocation structures in aluminum grain boundaries, *Phil. Mag.* A44 (1981) 1239–1254.
- [50] S. Namilae, N. Chandra, T.G. Nieh, Atomic simulation of grain boundary sliding in pure and magnesium doped aluminum bicrystals, *Scripta Mater.* 46 (2002) 49–54.
- [51] T. Hirata, T. Osa, H. Hosokawa, K. Higashi, Effects of flow stress and grain size on the evolution of grain boundary microstructure in superplastic 5083 aluminum alloy, *Mater. Trans.* 43 (2002) 2385–2391.
- [52] H. Somekawa, H. Watanabe, T. Mukai, Effect of solute atoms on grain boundary sliding in magnesium alloys, *Phil. Mag.* 94 (2014) 1345–1360.
- [53] T. Surholt, C.H.R. Herzig, Grain boundary self-diffusion in Cu polycrystals of different purity, *Acta Mater.* 45 (1997) 3817–3823.
- [54] J. Sommer, C.H.R. Herzig, T. Mushik, W. Gust, Temperature dependence and anisotropy of grain boundary self-diffusion along  $\Sigma<001>$  tilt boundaries in Ag, *Acta Metall. Mater.* 43 (1995) 1099–1107.
- [55] R. Schmelzle, B. Giakuplan, T. Muschik, W. Gust, R.A. Fournelle, Diffusion induced grain boundary migration of symmetric and asymmetric  $<001>$   $\{001\}$  tilt boundaries during the diffusion of Zn into Cu, *Acta Metall. Mater.* 40 (1992) 997–1007.
- [56] S.V. Divinski, G. Replitz, G. Wilde, Grain boundary self-diffusion in polycrystalline nickel of different purity levels, *Acta Mater.* 58 (2010) 386–395.
- [57] Q. Ma, R.W. Balluffi, Diffusion along  $[001]$  tilt boundaries in the Au/Ag system-I Experimental results, *Acta Metall. Mater.* 41 (1993) 133–141.
- [58] S.G. Song, G.T. Gray III, Structural interpretation of the nucleation and growth of deformation twins in Zr and Ti-1; Application of the coincidence site lattice theory to twinning problems in HCP structures, *Acta Metall. Mater.* 43 (1995) 2325–2337.
- [59] G.T. Gray III, High-strain-rate deformation: mechanical behavior and deformation substructures induced, *Annu. Rev. Mater. Res.* 42 (2012) 285–303.
- [60] M.R. Barnett, O. Bouaziz, L.S. Toth, A microstructure based analytical model for tensile twinning in a rod textured Mg alloy, *Int. J. Plast.* 72 (2015) 151–167.
- [61] S. Dong, Q. Yu, Y. Jiang, F. Wang, L. Jin, W. Ding, Characteristic cyclic plastic deformation in ZK60 magnesium alloy, *Int. J. Plast.* 91 (2017) 25–47.
- [62] T.G. Langdon, A unified approach to grain-boundary sliding in creep and superplasticity 42 (1994) 2437–2443.
- [63] H. Margolin, M.R. Stanescu, Polycrystalline strengthening, *Acta Metall.* 23 (1975) 1411–1418.
- [64] J.D. Licingston, B. Chalmers, Multiple slip in bicrystal deformation, *Acta Metall.* 5 (1957) 322–327.
- [65] R.E. Hook, J.P. Hirth, The deformation behavior of isoaxial bicrystals of Fe-3%Si, *Acta Metall.* 15 (1967) 535–551.
- [66] J. Koike, Enhanced deformation mechanisms by anisotropic plasticity in polycrystalline Mg alloys at room temperature, *Metal. Mater. Trans.* 36A (2005) 1689–1696.
- [67] M.F. Ashby, R.A. Verrall, Diffusion-accommodated flow and superplasticity, *Acta Metall.* 21 (1973) 149–163.
- [68] H. Somekawa, A. Singh, T. Mukai, Superplastic behavior in Mg-Zn-Y alloy with dispersed quasicrystalline phase particle, *Adv. Eng. Mater.* 11 (2009) 782–787.
- [69] Y. Chen, C.A. Schuh, Geometric considerations for diffusion in polycrystalline solids, *J. Appl. Phys.* 101 (2007), 063524.
- [70] A. Oudriss, J. Creus, J. Bouhattate, E. Conforto, C. Berziou, C. Savall, Feugas, Grain size and grain-boundary effects on diffusion and trapping of hydrogen in pure nickel, *Acta Mater.* 60 (2012) 6814–6828.
- [71] P. Mussor, C. Rey, A. Zaoul, Grain-boundary sliding and strain compatibility, *Res. Mech.* 14 (1985) 69–79.
- [72] R. Valiev, O.A. Kaibyshev, Mechanism of superplastic deformation in a magnesium alloy; Role of grain-boundaries, *Phys. Status Solidi A44* (1977) 477–484.
- [73] T. Matsunaga, T. Kameyama, S. Ueda, E. Sato, Grain boundary sliding during ambient-temperature creep in hexagonal close-packed metals, *Phil. Mag.* 90 (2010) 4041–4054.
- [74] H. Tonda, T. Kawasaki, Temperature dependence of  $\{11-22\}<-1-123>$  slip in zinc, *J. Jpn. Inst. Metals* 47 (1983) 284–293.
- [75] W.F. Gale, T.C. Totemeier, *Smithells Metals Reference Book*, Eight edition, Elsevier, 2004.
- [76] H.W. Son, J.W. Lee, S.K. Hyun, Mechanism of grain boundary serration during hot deformation of AZ31 alloy: role of grain boundary dislocations and grain boundary sliding, *Int. J. Plast.* 125 (2020) 118–132.
- [77] D. Ando, Y. Suto, J. Koike, Internal microstructure observation of enhanced grain-boundary sliding at room temperature in AZ31 magnesium alloy, *Mater. Sci. Eng. A666* (2016) 94–99.
- [78] H. Masuda, T. Kanazawa, H. Tobe, E. Sato, Dynamic anisotropic grain growth during superplasticity in Al-Mg-Mn alloy, *Scripta Mater.* 149 (2018) 84–87.
- [79] H. Masuda, E. Sato, Diffusional and dislocation accommodation mechanisms in superplastic materials, *Acta Mater.* 197 (2020) 235–252.